RAA 2016 Vol. **16** No. **7**, 104 (10pp) doi: 10.1088/1674–4527/16/7/104
http://www.raa-journal.org *http://iopscience.iop.org/raa*

***R**esearch in*
***A**stronomy and*
***A**strophysics*

Spectral lags of flaring events in LS I+61°303 from RXTE Observations

Tamal Sarkar[1,2], Samir Sarkar[1] and Arunava Bhadra[1]

[1] High Energy & Cosmic Ray Research Centre, University of North Bengal, Siliguri, WB 734013, India; *aru_bhadra@yahoo.com*
[2] University Science Instrumentation Centre, University of North Bengal, Siliguri, WB 734013, India

Received 2015 October 6; accepted 2016 March 14

Abstract This work reports the first discovery of (negative) spectral lags in X-ray emission below 10 keV from the gamma ray binary LS I+61°303 during large flaring episodes using Rossi X-ray Timing Explorer (RXTE) observations. It is found from the RXTE data that during the flares, low energy (3–5 keV) variations lead the higher energy (8–10 keV) variations by a few tens of seconds whereas no significant time lag is observed during the non-flaring states. The observed spectral lag features for flaring events suggest that inverse Compton scattering may be operating, at least in some part of the system. Another possibility is that the sites of particle acceleration may be different for flaring and non-flaring events such as in the microquasar model, in which the flaring radiation may come from hot spots sitting above the black hole while steady state emissions are due to the jets.

Key words: X-rays: binaries — X-rays: individual (LS I+61°303)

1 INTRODUCTION

Recently, the gamma ray binary system LS I+61°303 has drawn a lot of interest due to the fact that though it is one of the three known gamma-ray binaries detected in the entire energy range from radio to TeV and the system has been observed extensively, the nature of the compact object in the system, particularly whether it is a pulsar (neutron star) or a microquasar (black hole), is still not clear. In the former scenario (Maraschi & Treves 1981), the non-thermal emission from the source is expected to be powered by interaction between the stellar and pulsar winds whereas for the latter possibility (Taylor & Gregory 1984) the non-thermal emission is likely to be powered by accretion and jet ejection.

The presence of an extended jetlike and precessing radio emitting structure (Massi et al. 2001; Massi 2004) led to microquasar status of the source. However, a rotating elongated (cometary) morphology was noticed in VLBA images (Dhawan et al. 2006), which has been interpreted as due to the interaction between the relativistic wind of a pulsar and the wind of a companion Be star. Such a scenario receives support from recent VLBI observations (Moldón et al. 2012). However, no clear evidence for a jet (a signature for accretion) has been found so far, nor have any pulsations have been convincingly detected yet in deep radio (McSwain et al. 2011) and X-ray searches that could confirm the presence of a pulsar in the system. The emission mechanisms powering the system also remain uncertain. Recently, two short bursts have been observed from the direction of LS I+61°303 with SWIFT-BAT (Barthelmy et al. 2008; Torres et al. 2012) having characteristics typical of those observed in magnetars (strongly magnetized neutron stars), implying that the system may host a magnetar (Papitto et al. 2012).

Astronomical observations suggest that LS I+61°303 is a high-mass X-ray binary consisting of a low-mass $[M \sim (1-4)M_{\odot}]$ compact object orbiting around an early type rapidly rotating B0 Ve main sequence star with a stable equatorial shell along an eccentric $e \sim 0.7$ orbit (Gregory & Taylor 1978). The radio source GT 0236 +601 is considered to be associated with this Be star. The radio outbursts show a periodicity of about 26.496 days (Gregory & Taylor 1978) and a further modulation of the outburst phase and outburst peak flux with a (super-orbital) period of $\sim 1667 + / - 8$ days (Gregory 2002). The same orbital periodicity is also found in other bands - optical (Hutchings & Crampton 1981; Mendelson & Mazeh 1989), infrared (Paredes et al. 1994), soft X-rays (Paredes et al. 1997; Torres et al. 2010) and gamma rays from MeV (Massi 2004; Abdo et al. 2009) to TeV (Albert et al. 2006). TeV gamma rays are, however, only detected close to the apastron passage of the compact object in its orbit around the Be star.

A simple featureless absorbed power law in the X-ray energy band provides an effective fit to the observational spectral data from the source. Such a power law behavior continues in the MeV to GeV energy range with an exponential cutoff at 3.9 GeV as revealed from the Fermi-LAT observations (Hadasch et al. 2012; Abdo et al.

2009). An anti-correlation between flux and X-ray photon index was found in a long-term X-ray monitoring campaign of the system by the Rossi X-ray Timing Explorer (RXTE) mission (Li et al. 2011). Regarding temporal behavior, the X-ray observations conducted on LS I+61°303 showed extreme variation in the light curve on a kilosecond (ks) timescale between different orbital cycles: the flux is found to vary by a factor of about three over a single orbital cycle with a peak flux between orbital phases 0.4 and 0.6 (Goldoni & Mereghetti 1995; Taylor et al. 1996). A sharp decrease in the flux of the order of a factor of three over a time period of a few thousand seconds at an orbital phase 0.61 was noticed from an observational campaign of the system using XMM-Newton (Sidoli et al. 2006). It was further found that the hardness ratio (HR) changes with the change in flux. The presence of ks scale miniflares in the source, with emission increasing by a factor of two over a timespan of roughly 1 hour along with a correlation between harder emission and increased flux, was identified from the Chandra observations (0.3–10 keV) of LS I+61°303 near orbital phase 0.04 (Paredes et al. 2007).

Long term monitoring of the system was performed by the RXTE mission covering the period between 2006 October and 2010 September that included 42 adjacent cycles associated with orbital motion of the system (Li et al. 2011, 2012). Besides various important spectral and temporal behaviors of the system, the RXTE observations led to the discovery of related sub-ks scale flaring episodes. A total of five large flaring episodes were revealed from the RXTE observations which showed that the X-ray emission from the source changed by up to a factor of six over timescales of a few tens of seconds and the doubling times were as fast as 2 s (Smith et al. 2009; Li et al. 2011).

In this article, exploiting the RXTE observations of LS I+61°303, we have presented the results of the spectral time lag, i.e. the difference in times of arrival between high- and low-energy photons in the large flaring episodes. We shall show evidence that in the flaring episodes, the hard X-ray peak flare emission lags behind the soft X-ray emission with a time delay of a few tens of seconds. In contrast, during the steady (non-flaring) states, the spectral lag of the system is found to be consistent with zero lag. The implications of the present findings on the models of LS I+61°303 are discussed.

2 DATA REDUCTION

The RXTE Proportional Counter Array conducted long-term monitoring of LS I+61°303 covering 42 adjacent cycles of the 26.496 day binary orbital period between 2006 October and 2010 September and detected five flaring episodes with a timescale of a few hundred seconds. To study the spectral lag behavior of all the flares observed with RXTE and for spectral analysis, we follow the same data analysis method adopted in Smith et al. (2009); Li et al. (2012), i.e., light curves are generated using the "Good Xenon" mode (with resolution less than 16 s) from RXTE/PCA data whereas for spectral analysis the "Standard 2" mode was exploited. Data reduction was performed using HEASoft 6.12. We filtered the data using the standard RXTE/PCA criteria. The pcabackest has been used to generate a simulated background spectra/light curve (using Standard 2 mode) and PCA response matrices are obtained with pcarsp. The background light curve was subtracted from the Good Xenon observations by utilizing the FTOOLS routine lcmath. For the study of spectral lag in this work, we derived the light curves for two widely different energy intervals, 3–5 keV and 8–10 keV.

A proper choice of time binning is very important for extraction of spectral lags. Presumably, by changing the time binning of the light curve, one is affecting the signal-to-noise ratio. For very small time binning, the signal-to-noise ratio may become very small. On the other hand, the sought-after information from the light curve may be lost due to the use of overly large time bin sizes. Considering that the five flares observed by RXTE are binned into 5 s intervals, to estimate spectral lags in non-flaring (steady) episodes we select data sets for all the observations from event ID modified Julian date (MJD) 54345 to 54705 (a total of 141 observations) covering all the flaring episodes. Applying the cross-correlation function (CCF) technique, as discussed below, we estimate lags between the flare light curve at two different energies ($3-5$ and $8-10$ keV) for each observation.

For the study of spectral behavior, again we follow the procedure adopted in Smith et al. (2009), i.e. the standard quality criteria cuts are applied while selecting data, the Standard 2 mode (129 channels) is considered, the background spectra are simulated with pcabackest, the PCA response matrices are created using pcarsp and finally XSPEC12 is exploited to fit the background subtracted spectra in the energy interval 3–10 keV.

3 RESULTS

Five large flaring episodes, each with a duration of a few hundred seconds, have been observed by the RXTE mission (Table 1). The MJD 54356 is reported to be the most powerful of the observed flares with a flux $7.2 \pm 0.2 \times 10^{-11}$ erg s^{-1} cm^{-2}, which is larger than three times the average flux in the system. In contrast, the flux level of the system for non-flaring events is found to typically modulate between 0.5×10^{-11} and 2.0×10^{-11} erg s^{-1} cm^{-2} (Smith et al. 2009). Except for one (MJD 54372), all the flares are observed between 0.6 and 0.9 orbital phase bins of LS I+61°303, setting the phase to zero at Julian date (JD) 2 443 366.775 following the orbital solution by Casares et al. (2005). During flaring episodes 4 and 5, the spectral index varies with time and the flux exhibits a linear anti-correlation with spectral index as reported by Li et al. (2011).

An important question to address before applying spectral lag analysis is whether any real variability exists in the light curves considered here, i.e. the observed flares are not caused by the same stochastic process that produces variability in the rest of the light curve. To examine this, we

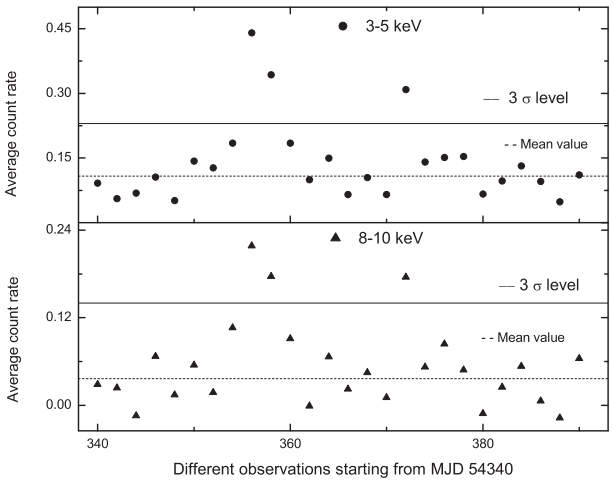

Fig. 1 Time (in MJD) variation of the count rate over the period MJD 54340 to MJD 54390 for two X-ray energies 3–5 keV (*upper panel*) and 8–10 keV (*lower panel*). The dashed lines denote the average count rate over the stated time period and the solid lines represent the 3σ count rate above the mean. The three flaring episodes, MJD 54356, MJD 54358 and MJD 54372, were detected with more than a 3σ significance level.

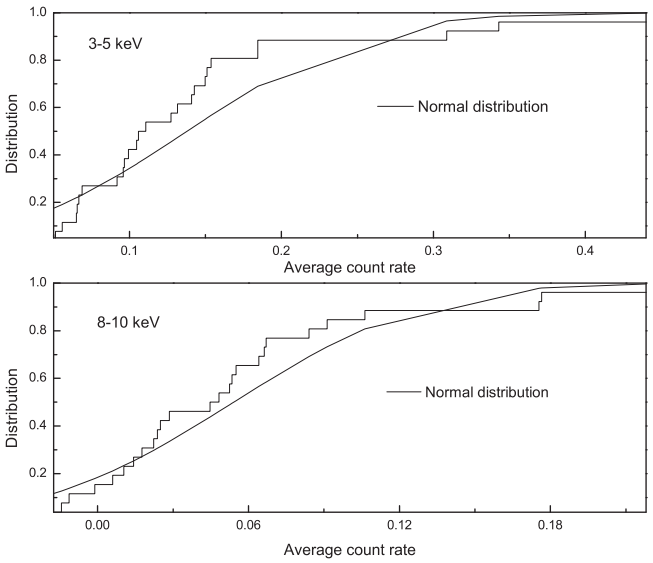

Fig. 2 The KS test with Lilliefors correction for the count rate over the period MJD 54340 to MJD 54390 for two X-ray energies 3–5 keV (*upper panel*) and 8–10 keV (*lower panel*). The p values are found to be < 0.01 and < 0.05 respectively for the energy bands 3–5 keV and 8–10 keV.

first compute the count rate in each observation (the RXTE mission took nearly 1 ks exposures every day over a period of 4 years) and plot the time variation of the count rate in two different energy bands, $3-5$ keV and $8-10$ keV as displayed in Figure 1, over the period MJD 54340 to MJD 54390. The count rates in the event IDs MJD 54356, 54358 and 54372 are found to be more than 3σ higher than the average count rate and thereby the events are identified as flaring episodes. We have also applied the Kolmogorov-Smirnov (KS) test with the Lilliefors correction (Lilliefors 1967) to check the variability. For this, we also consider the count rate for each observation over the period MJD 54340 to MJD 54390. The result is shown in Figure 2. Assuming the null distribution to be normal, the null hypothesis (the signals are not flares but simply Gaussian noise) is rejected with p values less than 0.01 and 0.05 respectively in energy bands $3-5$ keV and $8-10$ keV.

Each flaring episode contains several sub-flares with variability on the timescale of a few tens of seconds as has been (originally) demonstrated by Smith et al. (2009) and Li et al. (2011) from RXTE data. However, not all the sub-flares are well structured, having a clear rise and fall (Smith et al. 2009). To verify if the sub-flares within flaring episodes are real and not noise, we again employ the KS test with Lilliefors correction (Lilliefors 1967) as shown in Figure 3 for the flaring event ID MJD 54372. The confidence levels of the variability found from the KS test with Lilliefors correction for MJD 54356, MJD 54358 and MJD 54372 are $> 93\%$, $> 95\%$ and $> 99\%$ respectively in the energy band $3-5$ keV and $> 99\%$, $> 92\%$ and $> 99\%$ respectively in the energy band $8-10$ keV. The KS test of the flaring IDs thereby indicates that the sub-flares within flaring episodes are also real effects. We, therefore, proceed to study spectral lag for the flares.

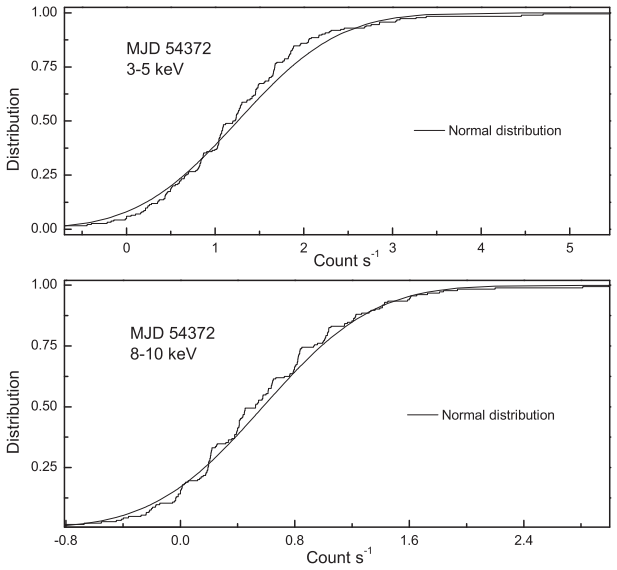

Fig. 3 The KS test with Lilliefors correction for the flaring event ID MJD 54372. The *upper* and *lower* panels correspond to energy windows $3-5$ keV and $8-10$ keV respectively.

For the purpose of estimating spectral lag, we need the presence of at least one well defined flare having clear rise and fall in light curves of both the considered energy bands ($3-5$ keV and $8-10$ keV). After imposing such conditions, we only found a few flaring events such as those given in Figures 4–5 for the event IDs MJD 54356 and MJD 54372 respectively.

Generally, spectral lag is extracted from either the pulse peak - fit method (Norris et al. 2005; Hakkila et al. 2008), or through the CCF analysis method (Link et al. 1993; Fenimore et al. 1995; Cheng et al. 1995; Norris et al.

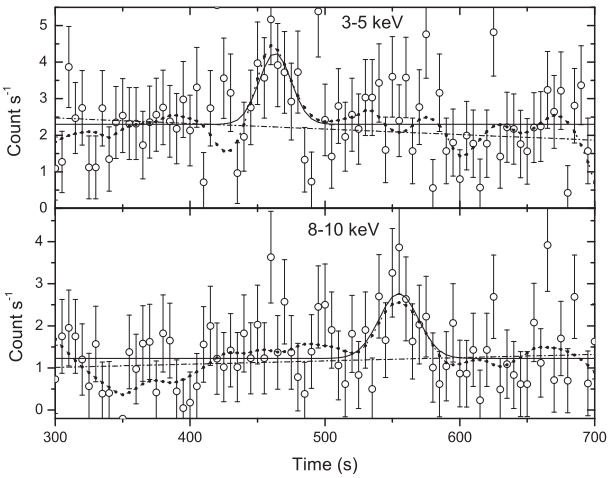

Fig. 4 The light curve of the flaring event ID MJD 54356 over the time window 300–700 s of the observation. The solid and dashed lines represent respectively the Gaussian fitting of the sub-flare and the smoothed line after application of the Loess method with the parameter $\alpha = 0.2$.

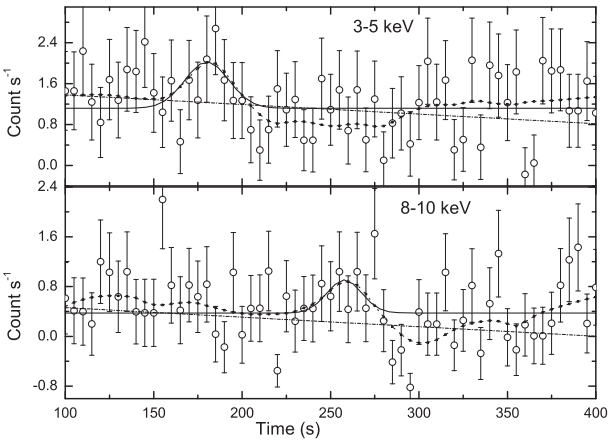

Fig. 5 Same as Fig. 4 but for the flaring event ID MJD 54372 over the time window 100–400 s of the observation.

2000). The former approach requires a certain pulse model for the pulses in the light curve. In the CCF analysis approach, the time delay corresponding to the global maximum of the CCF gives the spectral lag. The CCF between two energy bands has been calculated using the crosscor tool in Xrones (HEASOFT) and the normalization parameter is set (option 0) such that the count rates are normalized to the average rate.

We adopt both the mentioned techniques for estimation of spectral lag in the flaring events.

We first apply the direct CCF method. When we considered a longer time interval such as $300 - 700$ s for event ID MJD 54356, the significance of CCF is small, exhibiting noise like behavior which cannot be satisfactorily fitted by a Gaussian or other regular function. This is probably because here the light curve over a longer time interval is characterized by many 'emission events' rising or decaying on different timescales, thereby diluting the spectral lag characteristics. When we select marginal time intervals just

Table 1 The details of the flaring events observed by the RXTE mission over the energy range 3–10 keV. The phases have been determined by setting the phase to zero at JD 2 443 366.775.

Sl no.	Event ID MJD	Phase	Flux (erg s^{-1} cm^{-2})
1	54356	0.787	$7.2 \pm 0.2 \times 10^{-11}$
2	54358	0.861	$3.5^{+0.1}_{-0.2} \times 10^{-11}$
3	54372	0.379	$4.9^{+0.1}_{-0.2} \times 10^{-11}$
4	54670.84444	0.651	$(1 - 5) \times 10^{-11}$
5	54699.653333	0.739	$(2.5 - 10) \times 10^{-11}$

Table 2 Spectral Lags between Light Curves of $8 - 10$ keV and $3 - 5$ keV for the Flaring Events

Flaring events	Event ID (MJD)	Spectral lag by CCF (s)
1	54356	–16.2 ± 3.8
2	54372	–23.0 ± 6.6
3	54358	–2.2 ± 1.8
4	54670.844444	–5.8 ± 0.7
5	54699.653333	–1.1 ± 0.3

encircling a flare in the stated two energy bands (i.e. the time interval contains the flare in both the energy bands), we found a more regular CCF. For instance, we choose the time interval $420 - 600$ s in the case of MJD 54356 which contains relatively higher mean variance in both the energy ranges. After selection of time intervals, spectral lags are obtained as the time delay corresponding to the global maximum of the CCF. Gaussian fitting is used to locate the global maximum as shown in Figures 6–10 for the five flares. The estimated spectral lags are displayed in Table 2. Note that even after such time interval selection, we have not obtained a CCF with a regular shape for the flare in the case of event ID MJD 54358, and neither did we get a reasonable significance for the CCF. When we took smaller time bins, no regular behavior of CCF was observed. The reason is that the spectral delay is so much that the (small) time window does not contain the flare in both soft and hard band light curves. So, we come to the conclusion that in the present case, spectral lag only occurs for well defined flares, not for the continuum. The results are, however, robust in the sense that a small change of the time window (or sliding of the time window) by a few tens of seconds does not affect the spectral lag results much. For instance, in the case of MJD 54356, the choice of the time window $345 - 550$ s gives a spectral lag of 16.8 ± 1.02 s whereas the time window $450 - 700$ s produces a spectral lag of 16.18 ± 3.18 s which is almost the same as what we get (-16.2 ± 3.8) for the original time window of $420 - 600$ s. However, the significance of CCF is smaller for some other choices of the time window.

To estimate the spectral lags precisely for the well defined flares, we first smoothed the light curves of different energy bands using the 'Loess method' (Cleveland 1979; Cleveland & Devlin 1988) and then apply the CCF technique. It has been found that the use of the Loess filter provides a more reliable estimation of spectral lags for GRBs (Li & Chen 2012). Basically, it is a bi-variate smoothing

Table 3 Spectral Lags between Light Curves of $8-10$ keV and $3-5$ keV for Flaring Events

Flaring events	Event ID (MJD)	Spectral lag by CCF after Loess smoothing (s)	Spectral lag from Gaussian fitting
1	54356	–89.2 ± 0.8	–91.7 ± 2.7
2	54358	–101.0 ± 0.6	–110.1 ± 4.6
3	54372	–72.5 ± 0.4	–79.8 ± 4.7
4	54670.844444	–12.0 ± 0.6	–19.1 ± 4.3
5	54699.653333	–1.3 ± 0.2	–1.2 ± 2.9

procedure for drawing a smooth curve through a scatter diagram. In this method, the smooth curve is drawn in such a way that the value of the smoothed function at a particular location along the x-axis is only determined by the points in that vicinity and, locally, the curve minimizes the variance of the residuals. The Loess filter is characterized by a smoothing factor α that determines the smooth-span (in a data set with a total of N points, each smoothed value at the center of the smoothing span will be generated by a 2nd degree polynomial regression using linear least squares fitting with $N\alpha$ data points). Thus, the light curve will be less smoothed if α is small and vice versa. By trial and error, we take $\alpha = 0.2$ which gives the best fitting to the data points. We observed that for $\alpha \geq 0.3$, the regression function starts producing periodicity which is not present in the data. The flares or rather flaring pulses are clearly picked up by the Loess technique as can be seen, for example, in Figures 4 and 5 for flaring event IDs 54356 and 54372 respectively. Then we calculate the CCF between the smoothed curves at two energies as a function of time delay. For instance, the CCF between $8-10$ keV and $3-5$ keV for the flares of event ID MJD 54356 and event ID MJD 54372, as displayed in Figures 4 and 5, are shown in Figures 11 and 12 respectively. Subsequently, we estimated the spectral lag by Gaussian fitting of the region around the global maximum of the CCF. The calculated spectral lags by this technique are also displayed in Table 3. For $\alpha = 0.25$, we get almost the same spectral lag as that obtained with $\alpha = 0.2$.

In the absence of any definite pulse model for flaring events, we fit each of the flares at different energy bands with a Gaussian pulse. For instance, the fitted pulses (the solid lines) are displayed in Figures 4 and 5 in the energy bands $8-10$ keV and $3-5$ keV for the flares in observation IDs 54356 and 54372 respectively. Here, to ensure variability in light curves as well as to examine whether a Gaussian function reasonably describes the flare data, we fit the flare data with both a straight line and Gaussian curve and subsequently both the chi-square and F-test were applied.

Figure 13 demonstrates such a fitting for the flares in event ID MJD 54356. For a Gaussian fitting, the χ^2 values are found to be 0.88 and 0.61 (with a 5 s binning) respectively for $3-5$ keV and $8-10$ keV and for a 2 s binning, they become 0.78 and 1.10 respectively for energy bands $3-5$ keV and $8-10$ keV, which imply that a Gaussian distribution describes the data well. For MJD 54356, the F values are found to be 1.65 and 1.28 respectively for energy bands $3-5$ keV and $8-10$ keV when Gaussian fitted data and observed data are considered as samples, which are much smaller than the corresponding critical values of

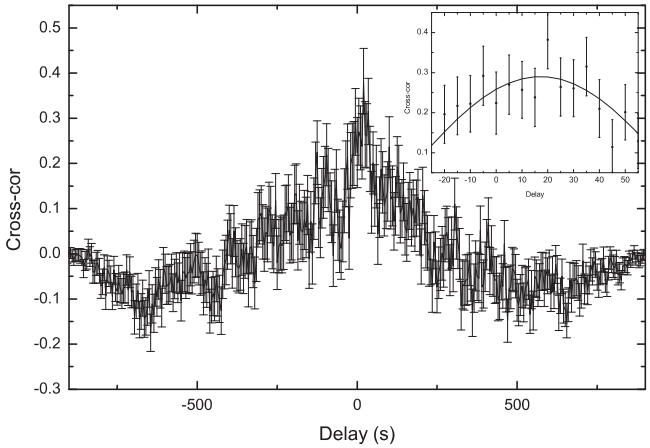

Fig. 6 The CCF between $8-10$ keV and $3-5$ keV light curves as a function of time delay for a flare in event ID MJD 54356 and the Gaussian fit of the peak region of the CCF.

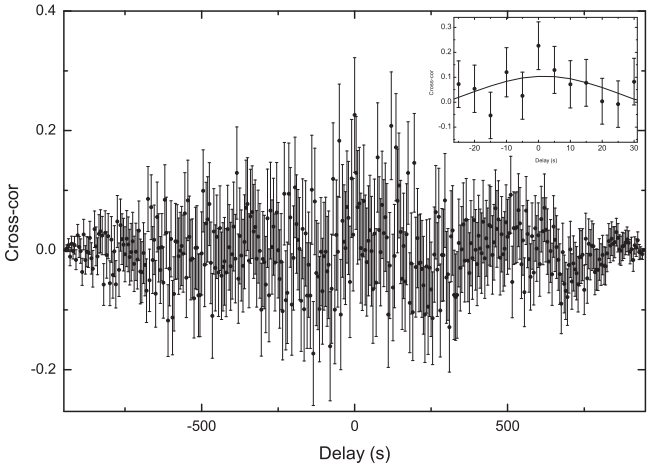

Fig. 7 Same as Fig. 6 but for the flaring event ID MJD 54358.

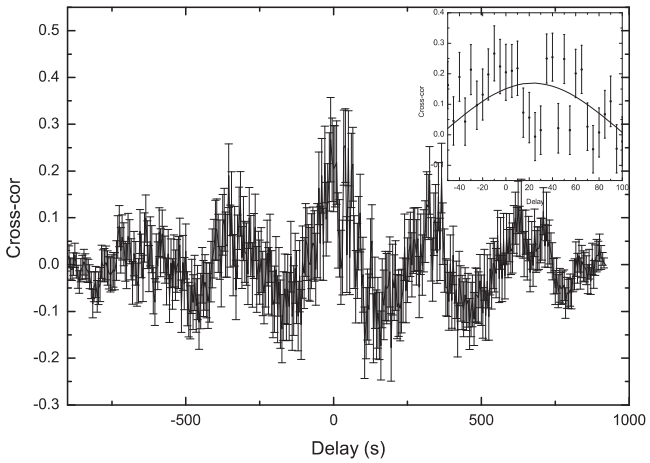

Fig. 8 Same as Fig. 6 but for the flaring event ID MJD 54372.

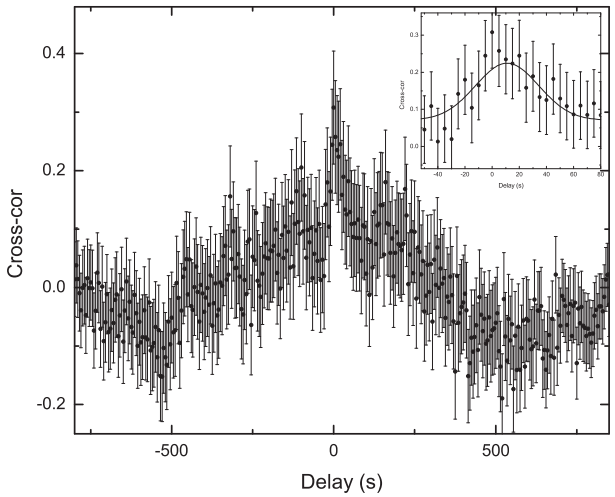

Fig. 9 Same as Fig. 6 but for the flaring event ID MJD 54670.844444.

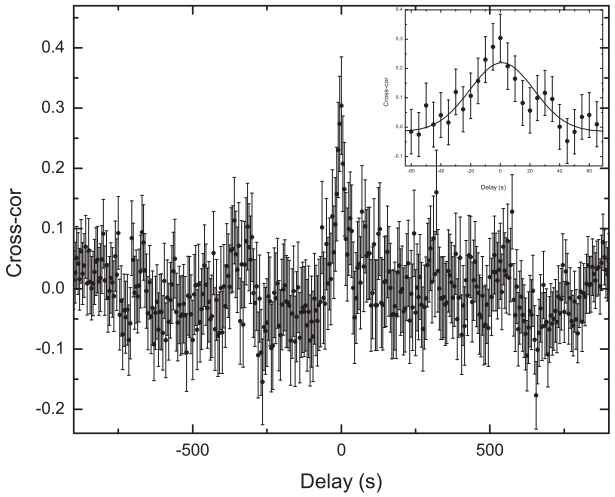

Fig. 10 Same as Fig. 6 but for the flaring event ID MJD 54699.653333.

F (2.22 and 2.27), unlike the case of fitting a straight line. For energy bands $3-5$ keV and $8-10$ keV the F values are 114.0 and 9.08 respectively when Gaussian fitted data and straight line fitted data of MJD 54372 are considered as samples. The corresponding critical values of F are 2.27 and 2.27. Thus we see that the observed flares can be reasonably described by a Gaussian function. From the fitted parameters we directly evaluate the spectral lag between $8-10$ keV and $3-5$ keV energy bands that are also given in Table 3. As we mentioned in Section 2, the choice of bin size is very important for studying the flares and thereby we have very limited scope to change the bin size. We have checked that the Gaussian description of the sub-flares for two bin sizes, 2 and 5 s, are satisfactory. It is found that the estimated parameters from Gaussian fitting, particularly the mean and standard deviation in the two different bin sizes, are quite close. For the spectral lag, the important parameter is the mean (xc). For the 2 s bin, xc equals 463.7 ± 1.5 and 559.7 ± 7.75 respectively for

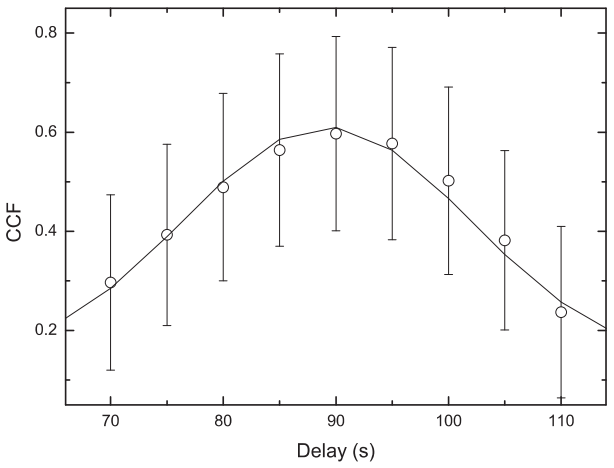

Fig. 11 Same as Fig. 6 but after Loess smoothing.

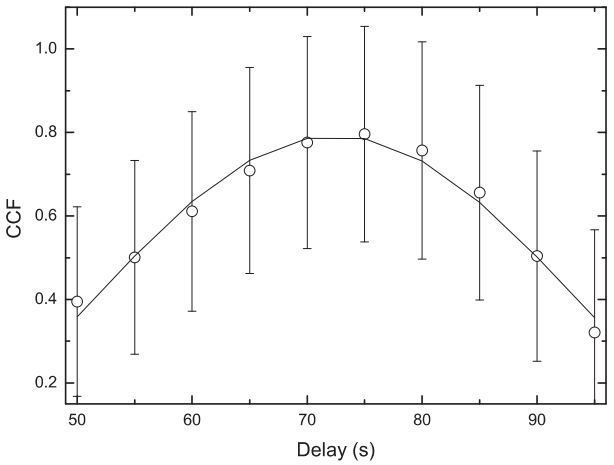

Fig. 12 Same as Fig. 6 but for the flaring event ID MJD 54372.

$3-5$ keV and $8-10$ keV whereas for the 5 s bin xc becomes 461.9 ± 1.1 and 555.5 ± 11.6 for $3-5$ keV and $8-10$ keV respectively. So, the estimated spectral lag is not affected much by the stated change in bin size in the present case.

The lag values obtained by the different techniques (CCF after Loess smoothing and pulse fitting) are found to be consistent with each other in all cases. The straightforward CCF gives a relatively smaller value for lags. The difference in the lags in the CCF analysis before and after smoothing seems to be due to noise. A well-defined flare is one which has a clear rise and fall. In the case of noise, one point may go up but the next point may go down. When the Loess method of smoothing is applied, at each point in the data set a low-degree polynomial is fitted using weighted least squares, giving more weight to points near the point and less weight to points further away. The value of the regression function for the point is then obtained by evaluating the local polynomial. So, fluctuations on both sides across the mean constant flux line are somewhat nullified with the use of Loess smoothing whereas the true flares are singled out. The CCF approach requires pulses in different energy bands to compare with and to identify the lag, if

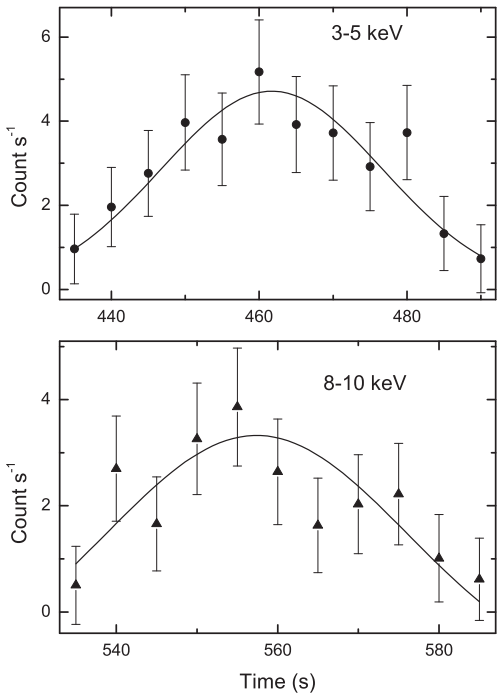

Fig. 13 Gaussian fitting of flare data in event ID MJD 54356 for two energy ranges, $3-5$ keV (*upper panel*) and $8-10$ keV (*lower panel*).

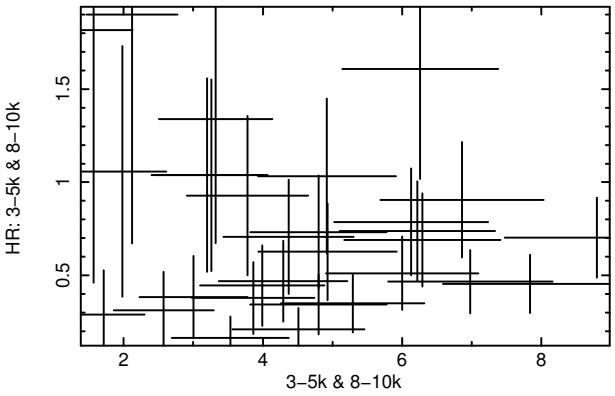

Fig. 14 Variation of HR with time for the event ID MJD 54356.

one is present. From constant flux lines, one cannot determine lag, so CCF after the Loess smoothing gives lag in flares of two different energy bands whereas direct CCF also considers the variability due to noise while evaluating lag. That is why direct CCF in the present case underestimates the lag. But importantly, all the methods suggest spectral lag. We noted that the spectral lags for the first three flaring episodes are substantially higher than the last two.

Spectral lag is usually caused by spectral hardening between the two spectra though such logic is not always valid (Roychoudhury et al. 2014). The study of HR provides a model-independent method to study the spectral hardening of a source. We calculate HRs for the flares between the light curve corresponding to $3-5$ keV and

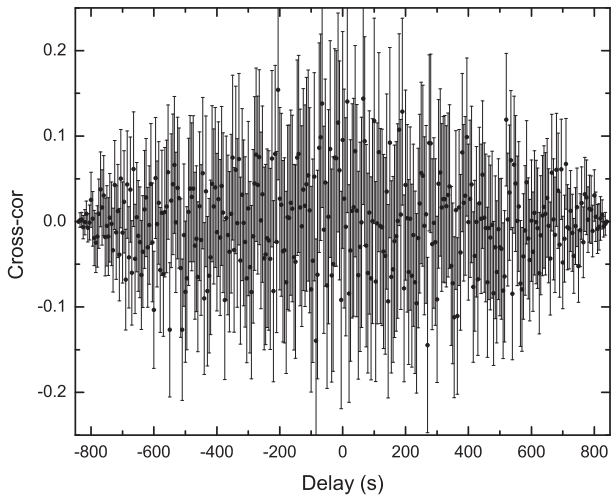

Fig. 15 Same as Fig. 6 but for the event ID MJD 54352.

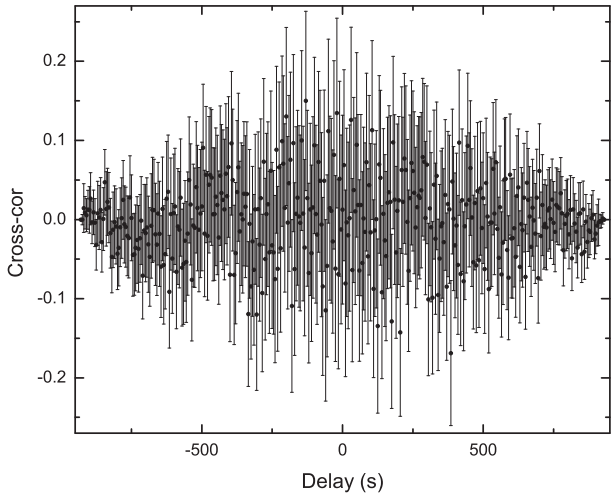

Fig. 16 Same as Fig. 6 but for the event ID MJD 54376.

$8-10$ keV. The variation of HR with time is displayed in Figure 14 for MJD 54356. However, due to large error bars associated with the points and limited statistics, no firm conclusion could be drawn from the time variation of HR due to spectral hardening.

Spectral lag estimation in the steady emission state is very difficult as there is no well defined spectral variation available for comparison between two different energy bands. So, we considered the light curves during the same time duration of 200 s at two different energies ($8-10$ and $3-5$ keV) for each observation ID and applied the direct CCF technique. Finally, the spectral lags are extracted from a Gaussian fit to the CCF (plotted as a function of time delay). However, we found that the significance of the CCF for non-flaring events is quite low, and neither have any regular shape as can be seen from Figures 15 and 16 for the event IDs MJD 54352 and 54376 respectively. If we still fit the CCFs by a Gaussian function, we found that the average spectral lag for the 141 observations between the event IDs MJD 54345 and 54705 is 0.01 ± 0.04 s and the

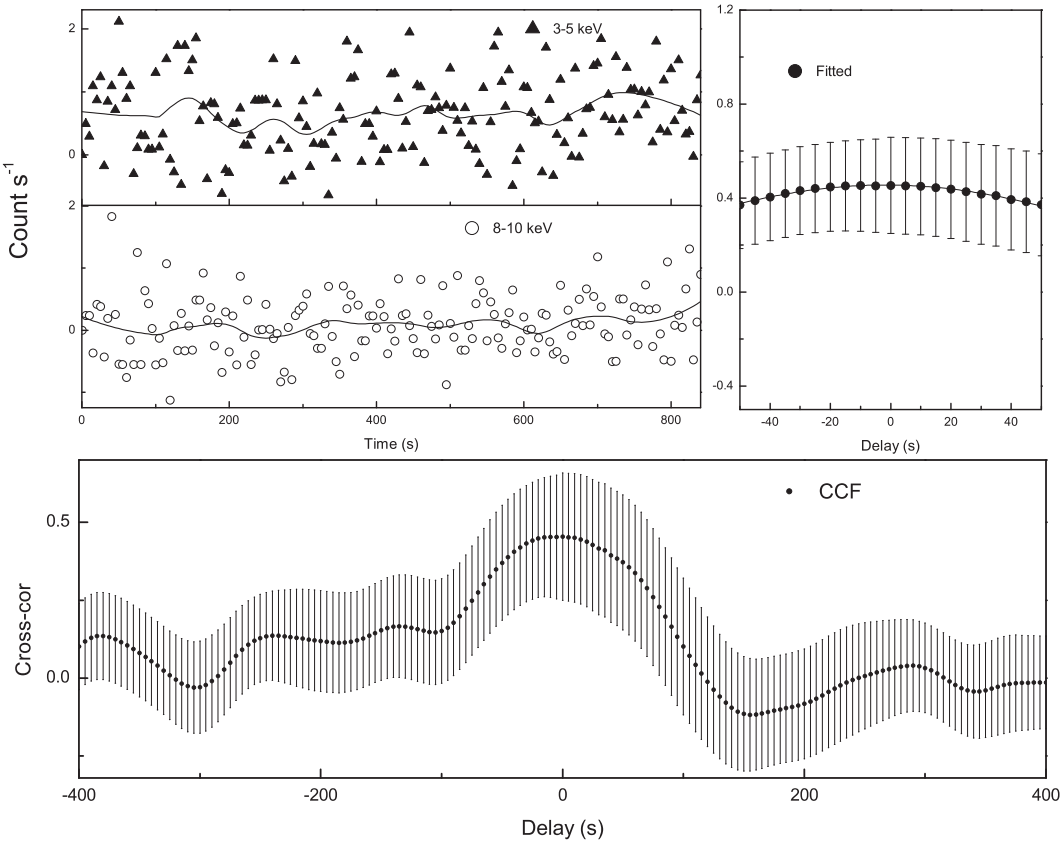

Fig. 17 Light curves of the event ID MJD 54352 at two energy bands, 3–5 keV (*upper left panel*) and 8–10 keV (*lower left panel*), with Loess smoothing (represented by the solid lines). The CCF after Loess smoothing is shown in the *bottom panel* whereas the Gaussian fitting of the peak of the CCF is shown in the *right panel*.

maximum spectral lags from direct CCF out of the 141 observations in the steady state are 4.9 ± 1.9 and 4.9 ± 1.5 s corresponding to the event IDs MJD 54352 and 54385 respectively. Here it is worth pointing out that due to poor correlation, no reliable estimate of lag is possible for non-flaring events from CCF studies. If Loess smoothing is applied, better correlation between light curves of two energies is noticed for non-flaring events, as also shown in Figure 17 for event ID MJD 54352 for instance (the corresponding lag becomes 0.4 ± 0.3 s). On application of the Loess method, it is found that spectral lags of all the steady emission events are more or less consistent with zero lag value.

4 DISCUSSION

A model of LS I+61°303 which reproduces the energy spectrum of the system should also be able to give the spectral lag behavior obtained here from the RXTE observations. The spectral data of the source are well described by a simple featureless absorbed power law, including the flaring events. Note that such spectral behavior (power law spectrum and negative lag) has been observed for Galactic (candidate) black hole binaries (in hard states) and also for AGNs (Uttley et al. 2011).

As mentioned before, there are mainly two competing models for LS I +61°303, the accretion driven (microquasar) and binary pulsar models. In the former (accretion driven) scenario, arising from the (companion) stellar wind-fed accretion disk, a jet is formed in which electrons are accelerated. These electrons are cooled down by the synchrotron process or by inverse Compton scattering of local stellar photons. In the pulsar model, the shock between the pulsar and stellar winds from the massive companion is responsible for acceleration of electrons. In the microquasar model of LS I+61°303, the observed 'miniflares' are due to fast variations in the stellar wind (Smith et al. 2009; Bosch-Ramon et al. 2005). A higher electron acceleration efficiency in the jets (and higher flux) is expected if there are sudden increases in accretion. This leads to a higher peak in the electron energy distribution and hence to a harder emission spectrum. To explain flares and flux variability on ks timescales in the framework of the binary pulsar model of the system, the clumsiness of the stellar wind is usually assumed; when the pulsar comes very close to the companion Be star and thereby is heavily exposed to the fast polar wind, clumps of relativistic electrons in the polar wind get mixed with the pulsar wind and are accelerated at the termination shocks of the pulsar wind (Zdziarski et al. 2010; Smith et al. 2009).

The observed spectral lag features for flaring events suggest that inverse Compton scattering might be operating in the system which accommodates both stated models. Since the time for rise and fall of the flares is just a few tens of seconds and doubling time is as small as 2 s (Smith et al. 2009), the observed variability of the system demands the emission region (D) should be less than 6×10^{10} cm unless it originated relativistically. An important point is whether within this timescale clumps can cool electrons via the inverse Compton process. In the binary pulsar model, the escape timescale of the pulsar wind mixed with the stellar wind is $t_{\rm esc} \sim D/v_{\rm wind}$ where $v_{\rm wind}$ can be taken to be equal to the terminal velocity of the equatorial wind, which is typically a few $100\ {\rm km\ s^{-1}}$ (Rea et al. 2010). A detailed analysis suggests that the inverse Compton losses of about 10 MeV electrons, which will lead to inverse Compton emission of X-ray photons between 1 and 10 keV, are likely to dominate at the inner region of the system unless the magnetic field in the inner region is not too high compared to its value in the pulsar wind nebula of ~ 1 G (Rea et al. 2010). In the outer part, synchrotron emission is expected to lead and contribute dominantly to the overall X-ray emission from the system (Rea et al. 2010). The observed negative spectral lag of flares in the system support such a picture if the flares are generated in the inner part of the system. In the framework of a microquasar model, the observed flaring radiation could be due to the emission from hot spots sitting above the black hole (compact object) while steady state emissions are due to the jets.

One also cannot rule out the possibility that the flaring events observed by the RXTE mission are not associated with the LS I+61°303 system (Li et al. 2011). Because of the large field of view of the PCA detector of LAXPC, such a probability exists. The observed significantly different spectral lags during flaring episodes are consistent with such a scenario of a different source for the origin of flaring and steady emission states from the direction of the system.

5 CONCLUSIONS

A study of spectral lag provides important understanding of the radiation mechanisms operating in an astrophysical object (for instance Roychoudhury et al. 2014). Study of the spectral lag in LS I+61°303 provides few very interesting results. From the RXTE observed data, we found for the first time that during the flares, low energy variations lead the higher energy variations, i.e. spectral lag is negative whereas there is almost no time lag during the steady (non-flaring) states, though accuracies of spectral time lags in the steady state are quite limited. For flares lasting a hundred seconds or so, spectral lags of a few tens of seconds between emission of $3-5$ keV and $8-10$ keV should be considered to be quite large. Any viable model of LS I+61°303 needs to explain such spectral lag behavior associated with this system.

In a recent work, it has been found that periodic radio flares, from the system, lag the X-ray flare by a phase of nearly 0.2, which is equivalent to a delay of 4.58×10^5 s. Such a feature is explained in terms of the time of flight of energetic electrons from the binary system to the radio emission region (Chernyakova et al. 2012). However, the spectral lag found in this work between emission of $3-5$ keV and $8-10$ keV cannot be ascribed to time of flight delay but rather is most likely related to the emission mechanism and thus the information should be helpful in understanding the nature of the source.

Acknowledgements The authors are thankful to an anonymous reviewer for insightful comments and suggestions that helped us to improve the manuscript.

References

Abdo, A. A., Ackermann, M., Ajello, M., et al. 2009, ApJ, 701, L123
Albert, J., Aliu, E., Anderhub, H., et al. 2006, Science, 312, 1771
Barthelmy, S. D., Baumgartner, W., Cummings, J., et al. 2008, GRB Coordinates Network, 8215
Bosch-Ramon, V., Paredes, J. M., Ribó, M., et al. 2005, ApJ, 628, 388
Casares, J., Ribó, M., Ribas, I., et al. 2005, MNRAS, 364, 899
Cheng, L. X., Ma, Y. Q., Cheng, K. S., Lu, T., & Zhou, Y. Y. 1995, A&A, 300, 746
Chernyakova, M., Neronov, A., Molkov, S., et al. 2012, ApJ, 747, L29
Cleveland, W. S. 1979, Journal of the American statistical association, 74, 829
Cleveland, W. S., & Devlin, S. J. 1988, Journal of the American statistical association, 83, 596
Dhawan, V., Mioduszewski, A., & Rupen, M. 2006, in VI Microquasar Workshop: Microquasars and Beyond, 52.1
Fenimore, E. E., in 't Zand, J. J. M., Norris, J. P., Bonnell, J. T., & Nemiroff, R. J. 1995, ApJ, 448, L101
Goldoni, P., & Mereghetti, S. 1995, A&A, 299, 751
Gregory, P. C., & Taylor, A. R. 1978, Nature, 272, 704
Gregory, P. C. 2002, ApJ, 575, 427
Hadasch, D., Torres, D. F., Tanaka, T., et al. 2012, ApJ, 749, 54
Hakkila, J., Giblin, T. W., Norris, J. P., Fragile, P. C., & Bonnell, J. T. 2008, ApJ, 677, L81
Hutchings, J. B., & Crampton, D. 1981, PASP, 93, 486
Li, J., Torres, D. F., Zhang, S., et al. 2011, ApJ, 733, 89
Li, J., Torres, D. F., Zhang, S., et al. 2012, ApJ, 744, L13
Li, Z., & Chen, L. 2012, PASP, 124, 297
Lilliefors, H. W. 1967, Journal of the American Statistical Association, 62, 399
Link, B., Epstein, R. I., & Priedhorsky, W. C. 1993, ApJ, 408, L81
Maraschi, L., & Treves, A. 1981, MNRAS, 194, 1P
Massi, M. 2004, A&A, 422, 267
Massi, M., Ribó, M., Paredes, J. M., et al. 2001, A&A, 376, 217

McSwain, M. V., Ray, P. S., Ransom, S. M., et al. 2011, ApJ, 738, 105
Mendelson, H., & Mazeh, T. 1989, MNRAS, 239, 733
Moldón, J., Ribó, M., & Paredes, J. M. 2012, in American Institute of Physics Conference Series, 1505, eds. F. A. Aharonian, W. Hofmann, & F. M. Rieger, 386
Norris, J. P., Marani, G. F., & Bonnell, J. T. 2000, ApJ, 534, 248
Norris, J. P., Bonnell, J. T., Kazanas, D., et al. 2005, ApJ, 627, 324
Papitto, A., Torres, D. F., & Rea, N. 2012, ApJ, 756, 188
Paredes, J. M., Marziani, P., Marti, J., et al. 1994, A&A, 288, 519
Paredes, J. M., Marti, J., Peracaula, M., & Ribo, M. 1997, A&A, 320, L25
Paredes, J. M., Ribó, M., Bosch-Ramon, V., et al. 2007, ApJ, 664, L39
Rea, N., Torres, D. F., van der Klis, M., et al. 2010, MNRAS, 405, 2206
Roychoudhury, A., Sarkar, S. K., & Bhadra, A. 2014, ApJ, 782, 105
Sidoli, L., Pellizzoni, A., Vercellone, S., et al. 2006, A&A, 459, 901
Smith, A., Kaaret, P., Holder, J., et al. 2009, ApJ, 693, 1621
Taylor, A. R., & Gregory, P. C. 1984, ApJ, 283, 273
Taylor, A. R., Young, G., Peracaula, M., et al. 1996, A&A, 305, 817
Torres, D. F., Rea, N., Esposito, P., et al. 2012, ApJ, 744, 106
Torres, D. F., Zhang, S., Li, J., et al. 2010, ApJ, 719, L104
Uttley, P., Wilkinson, T., Cassatella, P., et al. 2011, MNRAS, 414, L60
Zdziarski, A. A., Neronov, A., & Chernyakova, M. 2010, MNRAS, 403, 1873